Environmental Pollution 256 (2020) 113000

Contents lists available at ScienceDirect

Environmental Pollution

journal homepage: www.elsevier.com/locate/envpol

A 3D-hydrodynamic model for predicting the environmental fate of chemical pollutants in Xiamen Bay, southeast China

Liya Ma [a], Bin-Le Lin [b], Can Chen [a], Fumio Horiguchi [b], Tomomi Eriguchi [c], Yongyu Li [a], Xinhong Wang [a], *

[a] State Key Laboratory of Marine Environmental Science, Key Laboratory of the Coastal and Wetland Ecosystems, Ministry of Education, College of the Environment & Ecology, Xiamen University, Xiamen 361102, China
[b] Research Institute of Science for Safety and Sustainability, National Institute of Advanced Industrial Science and Technology (AIST), Japan
[c] Technical Research, Department Science and Technology Co., LTD., Japan

ARTICLE INFO

Article history:
Received 29 January 2019
Received in revised form
5 April 2019
Accepted 22 April 2019
Available online 13 November 2019

Keywords:
Hydrodynamic model
Xiamen Bay
Chemical pollutants
Environmental fate
Numerical simulation

ABSTRACT

Simulation model is very essential for predicting the environmental fate and the potential environmental consequences of chemical pollutants including those from accidental chemical spills. However very few of such simulation model is seen related to Chinese costal water body. As the first step toward our final goal to develop a simulation model for the prediction and the risk assessment of chemical pollutants in Chinese coastal water, this study developed a three-dimensional (3D) hydrodynamic model of Xiamen Bay (XMB). This hydrodynamic model was externally derived by meteorological data, river discharge and boundary conditions of XMB. We used the model to calculate the physical factors, especially water temperature, salinity and flow field, from June to September 2016 in XMB. The results demonstrated a good match between observations and simulations, which underscores the feasibility of this model in predicting the spatial-temporal concentration of chemical pollutants in the coastal water of XMB. Longitudinal salinity distributions and the mixing profile of river-sea interactions are discussed, including the obvious gradation of salinity from the river towards sea sites shown by the model. We further assumed that 1000 kg and 1000 mg/L of a virtual chemical pollutant leaked out from Jiulong River (JR) estuary (point source) and whole XMB (non-point source), respectively. The model illustrates that it takes three months for XMB to become purified when point source pollution occurs in the estuary, while half a year to be required in the case of non-point source pollution across the entire bay. Moreover, the model indicated that pollutants can easily accumulate in the western coastal zone and narrow waters like Maluan Bay, which can guide environmental protection strategies.

© 2019 Elsevier Ltd. All rights reserved.

1. Introduction

Xiamen Bay (XMB), surrounding the Xiamen Special Economic Zone of China, is an important external port on the southeast coast, and a typical semi-closed bay that receives the largest annual inputs of the Jiulong River (JR). Xiamen has growing concerns as an international port and scenic tourist city, both which require a healthy coastal environment. Numerous existing studies reveal that XMB has been polluted to a certain extent owing to rapid development and advanced manufacturing. Chemical pollutants such as pesticides as well as PCBs (polychlorinated biphenyls) one of the representative persistent organic pollutants, widely used in agriculture and commerce, respectively, are found in varying degrees in seafood from XMB, which poses a large risk to the district (Qian et al., 2017). Dichloro-Diphenyl-Trichloroethane (DDT), for example, was assessed in biota from warm regions in China, revealing that XMB, where the usage of pesticides in the region is same to the major agricultural provinces, is sorted into one of the worst categories (Grung et al., 2015). Coastal water such as XMB bears the pressure of chemical pollutants delivered by rivers, and thus persistent organic pollutants (Chau, 2005; Yuan et al., 2001; Hao et al., 2015; Cai et al., 2016) and heavy metal pollution issues across multiple phases (Li et al., 2013) have emerged in the XMB area. The JR is the second largest river in Fujian province, which discharges primarily into the XMB followed by Tong'an Bay and the Maluan Wan. Years of monitoring results show that the JR is the

---

* Corresponding author.
E-mail address: xhwang@xmu.edu.cn (X. Wang).

https://doi.org/10.1016/j.envpol.2019.113000
0269-7491/© 2019 Elsevier Ltd. All rights reserved.

main source of dissolved inorganic nitrogen (DIN) and other contaminants to XMB (Chen et al., 2013). The JR estuary, in the upper reaches of XMB, is a complex transition area where circulation and mixing processes vary with respect to specific environmental variables. It is therefore critical to examine both XMB and the JR estuary to solve the aquatic pollution issues related to chemical pollutants facing the Xiamen region. To examine these issues in real-time continuous monitoring is necessary, however current routine monitoring by government agencies occurs only once per day or per month and includes only surface waters, and cannot satisfy three-dimensional predictions and timely forecasts. Therefore, continuous and multilayered numerical simulations of the concentration of the chemical pollutants in the water of XMB and JR estuary is essential, which overcomes the time and labor constraints of continuous monitoring and on-site measurements.

With the aim of achieving the efficient monitoring in coastal water, a large effort has been made towards model simulations (Kim et al., 2018). Wang et al. (2017) developed a wave forecasting model to predict the height, cycle and direction of Xiamen bay waves. Zhai et al. (2017) utilized a hydrodynamic model coupled with a water quality module to successfully simulate flow and pollutant change considering the impact of a dam and runoff changes from anthropogenic interference in the Huai River. Lin et al. (2017) applied a two-dimensional model utilizing element technique and semi-implicit scheme to validate the primary water currents and exchange potential in Sansha Bay. The Marine environmental committee ocean model for freshwater was used to describe three salinity fronts and currents in the JR estuary that are highly sensitive to tidal fluctuations and topographic factors (Luo et al., 2012). The definition of “water age” was applied by using tide and wind data as the dominant factors influencing river flow process in the Liao River Estuary (Liu et al., 2017). Periáñez (2009) combined a barometric pressure model for residual flow, a barotropic model for tides and a sediment transport model to examine the spread of heavy metals such as Zinc (Zn) and Copper (Cu) in The Gulf of Cadiz. Nutrient levels of the Peer-Bazar River were estimated by the FLOW-3D mathematical model and Hydrological Engineering Center’s River Analysis System (HEC-RAS), to prevent further environmental degradation and re-establish control in this district (Homami et al., 2017). However, despite this body of work, limited studies have been seen on simulation model that can predict the environmental fate and the potential environmental consequences of chemical pollutants including those from accidental chemical spills by showing its spatial-temporal concentration and risk in Chinese coastal water. The incident of aromatic hydrocarbon (C9) spill happened on November 4, 2018 at Quanzhou bay (Fujian China) arises an urgent issue on the model simulation. This study, as the first step toward the final goal of developing a model for the prediction and the risk assessment of chemical pollutants in Chinese coastal water, we selected XMB, a typical semi-closed bay with our over years monitoring experience as the target case. We developed a 3D hydrodynamic model that can well simulate XMB coastal water driven by the physical parameters such as tides, depth, wind, river discharge and meteorological data of XMB.

2. Methodology

2.1. Model development

We developed XMB model based on the model framework of Tokyo Bay, Japan (Horiguchi et al., 2001). More detail information on the scheme of the model was shown in No. 1 supplementary material. The model of Tokyo Bay has been well approved and applied in a series risk assessment of chemical pollutants in Japan (e.g., Kobayashi et al., 2006). Moreover, Tokyo bay is a semi-closed bay located southeast of the Tokyo Metropolis. The situation from the viewpoints of geographical, hydrodynamical and pollutant catchment is quite similar to XMB. Fig. 1 shows the study area of XMB. It spans longitudinally from 117°49′ E to 118°21′ E, and latitudinally from 24°43′ N to 24°11′ N, eastward to Jinmen and west to the JR, encompassing the main administrative regions of Xiamen city. We divided this area into 3060 grids, each grid representing 1 km × 1 km of the coastal water in spatial. The details of the required physical parameters and the data collected in the coastal water for developing XMB model are summarized in Table 1. For the hydrodynamic modeling, meteorological data from inland Xiamen, discharge from three JR Harbors, initial temperature and salinity data of boundary areas and the river harbors, data of tides depth, and wind in the area are required (Table 1). To obtain the multiple-layer continuous full-coverage physical parameters used for the development of model, we firstly investigate and accumulate the current available monitoring data and then using a series of empirical equations to convert the limited instantaneous monitoring data into hourly values of each grid and layer. Detailed information on the conversion of the multiple-layer continuous full-coverage physical parameters was shown in No. 2 supplementary material.

To simulate the hydrodynamic condition of XMB, several main equations were used by referring to the model framework of Tokyo Bay (Horiguchi et al., 2001). The following equations were used for describing the motion (Eq. (1)), the continuity (Eq. (2)), the free surface (Eq. (3)), the heat conservation (Eq. (4)), the salinity (Eq. (5)), the state for seawater (Eqs. (6a)–(6f)) of XMB, respectively.

$$\frac{\partial v}{\partial t}+(v\cdot\nabla)v+w\frac{\partial v}{\partial z}+f_0k\cdot v=-g\nabla\zeta-\frac{g}{\rho_0}\int_{-H}^{0}\nabla\rho\,d_z+[\nabla\cdot(A_H\nabla)]v+\frac{\partial}{\partial z}\left(A_Z\frac{\partial v}{\partial z}\right)\tag{1}$$

$$\nabla\cdot v+\frac{\partial w}{\partial z}=0\tag{2}$$

$$\frac{\partial\zeta}{\partial t}+\nabla\cdot\left(\int_{-H}^{\zeta}vdz\right)=0\tag{3}$$

$$\frac{\partial T}{\partial t}+(v\cdot\nabla)T+w\frac{\partial T}{\partial z}=[\nabla\cdot(K_H\nabla)]T+\frac{\partial}{\partial z}\left(K_z\frac{\partial T}{\partial z}\right)\tag{4}$$

$$\frac{\partial S}{\partial t}+(v\cdot\nabla)S+w\frac{\partial S}{\partial z}=[\nabla\cdot(D_H\nabla)]S+\frac{\partial}{\partial z}\left(D_z\frac{\partial S}{\partial z}\right)\tag{5}$$

$$\rho=\frac{\sigma_t}{1000}+1\tag{6a}$$

$$\sigma_t=\sum_t+(\sigma_0+0.1324)\{1-A_t+B_t(\sigma_0-0.1324)\}\tag{6b}$$

$$\sigma_0=-0.069+1.4708S-0.00157S^2+0.0000398S^3\tag{6c}$$

$$\sum_t=-\frac{(T-3.98)^2}{503.570}\cdot\frac{T+28.30}{T+67.26}\tag{6d}$$

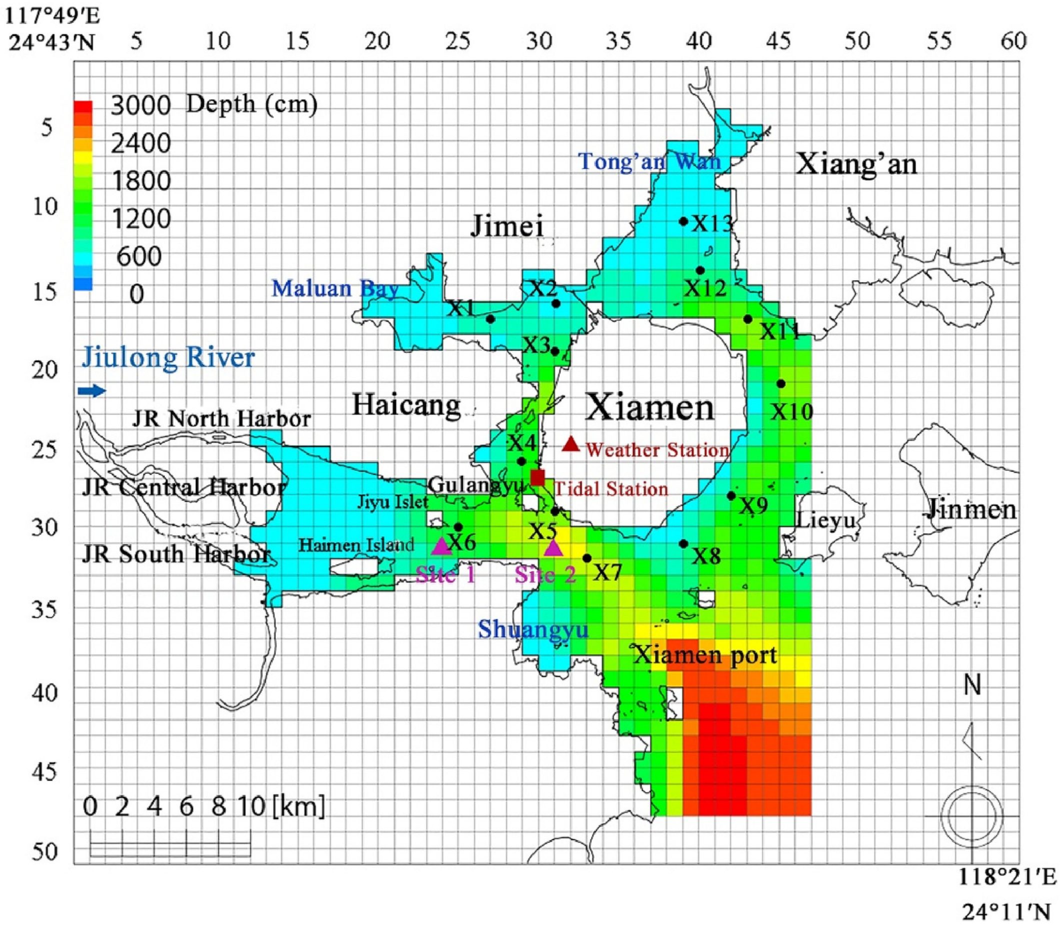
117°49′E
24°43′N
5
10
15
20
25
30
35
40
45
50
55
60
3000 Depth (cm)
2400
1800
1200
600
0
Tong'an Wan
Xiang'an
Jimei
Maluan Bay
X1
X2
X3
X4
X5
X6
X7
X8
X9
X10
X11
X12
X13
Jiulong River
JR North Harbor
Haicang
Xiamen
Weather Station
JR Central Harbor
Gulangyu
Tidal Station
Jiyu Islet
Lieyu
Jinmen
JR South Harbor
Haimen Island
Site 1
Site 2
Shuangyu
Xiamen port
N
0 2 4 6 8 10 [km]
118°21′E
24°11′N

Fig. 1. The study area of Xiamen Bay (XMB). Data was collected from three Jiulong River (JR) harbors, thirteen observation sites (X1-X13), a weather station (▲), a tidal station (■), target grids from Sites 1 and 2 for further vertical analysis (▲).

Table 1
The study area and the data used in developing XMB hydrodynamic model.

Content	Values
Study area	Xiamen Bay (XMB) (in Fig. 1)
Grids	51 (North-South) × 60 (West-East)
Grid unit	1 km
Layers in depth	Level 1: Surface to −5 m Level 2: 5 m to −10 m Level 3: 10 m to −15 m Level 4: 15 m to −20 m Level 5: 20 m to −30 m
Tide	Tidal Station (in Fig. 1)
Meteorological data	Air temperature, Cloud, Wind, Relative humidity in Weather Station (in Fig. 1)
Solar radiation and cloud amount	Xiamen University Siming Campus (118°5′ E, 24°26′ N)
Watershed conditions	3 rivers from JR North, Central and South Harbor (in Fig. 1)
Observed values for model validation	X1-X13 (Xiamen EPA, in Fig. 1)
Coordinate of longitudinal inspection point	Site 1 (24,31); Site 2 (31,31)
Coriolis parameter	$6.04 \times 10^{-5}\ \mathrm{s}^{-1}$
Horizontal eddy viscosity and diffusivity	$30\ \mathrm{m}^2\mathrm{s}^{-1}$
Vertical eddy viscosity and diffusivity	$30\ \mathrm{m}^2\mathrm{s}^{-1}$
Model simulation period	From June to September in 2016

$$A_t = T\left(4.7869 - 0.098185T + 0.0010843T^2\right) \times 10^{-3} \tag{6e}$$

$$B_t = T\left(18.03 - 0.8164T + 0.01667T^2\right) \times 10^{-6} \tag{6f}$$

where v is the transverse velocity, t is time, ∇ is the operator of the two-dimensional model, w is perpendicular velocity, z is the perpendicular coordination, k is the perpendicular unit vector, g is gravitational acceleration, ζ is the height between the sea surface and the mean sea level, ρ is the density of the water body, H is the height between the mean sea level and the bottom, A_H and A_Z are the moduli for transverse and perpendicular diffusion of momentum, respectively, f_0 is the Coriolis parameter (later described), and ρ_0 is density with the Boussinesq approximation, T is the temperature, S is the salinity. KH and KZ are the moduli for transverse and perpendicular diffusion of heat, respectively, and DH and DZ are the moduli for transverse and perpendicular diffusion of salinity, respectively.

The boundary conditions of XMB were described by Eqs. (7)–(9) for the surface and Eqs. (10) and (11) for the bottom, respectively (Horiguchi et al., 2001).

$$\frac{1}{\rho}\tau_x^S = \frac{\rho_a}{\rho}\gamma_a^2 W_x \sqrt{W_x^2 + W_y^2} \tag{7}$$

$$\frac{1}{\rho}\tau_y^S=\frac{\rho_a}{\rho}\gamma_a^2 W_y\sqrt{W_x^2+W_y^2} \tag{8}$$

$$\rho\cdot c\cdot \kappa\frac{\partial T}{\partial z}=Q \tag{9}$$

$$\frac{1}{\rho}\tau_x^B=\gamma_B^2 u_k\sqrt{u_k^2+v_k^2} \tag{10}$$

$$\frac{1}{\rho}\tau_y^B=\gamma_B^2 v_k\sqrt{u_k^2+v_k^2} \tag{11}$$

where τ_s is the wind stress vector, ρ_a is the density of air, γ_a^2 is the resistance modulus, W_x and W_y are wind speed in the x and y directions, respectively, c is the heat of seawater, κ is the Karman constant, Q is the downward heat flux. τ_x^B, τ_y^B is the friction of the bottom, and u_k, v_k is current speed in the x, y direction. No heat and salinity fluxes occur across the bottom layer.

The vertical eddy diffusivity and eddy viscosity in coastal regions is described by Eqs. (12) and (13) (Horiguchi et al., 2001).

$$\begin{aligned}\frac{\partial}{\partial t}(h_k e_k)=&-\frac{\partial}{\partial x}(M_k e_k)-\frac{\partial}{\partial y}(N_k e_k)-(\omega e)|_{z=-H_{k-1}}+(\mathrm{we})|_{z=-H_k}\\&+\frac{\partial}{\partial x}\left(h_k D_x\frac{\partial e_k}{\partial x}\right)+\frac{\partial}{\partial y}\left(h_k D_{\mathrm{yk=coastal\ region\ model}}\frac{\partial e_k}{\partial y}\right)\\&-\left(E_e\frac{\partial e}{\partial z}\right)|_{z=-H_{k-1}}+\left(E_e\frac{\partial e}{\partial z}\right)|_{z=-H_k}+S_e^k-D_e^k\end{aligned} \tag{12}$$

where $R_i=-\frac{g}{p}\frac{\partial\rho}{\partial z}/\left(\frac{\partial u}{\partial z}\right)^2$; $\varepsilon=\mathrm{L}\sqrt{e}$; $\mathrm{L}=k'z\sqrt{1-z/H}$

$$\mathrm{E}=\rho L\sqrt{e}\cdot exp\left\{m\frac{gL^2}{\rho\ e}\frac{\partial\rho}{\partial z}\right\} \tag{13}$$

where R_i is the Richardson number, ε is the perpendicular momentum transfer modulus, e is the sub-grid scale (SGS) energy, L is the length scale, z is the distance from the bottom, H is depth, E is the momentum perpendicular exchange modulus, D_x and $D_{\mathrm{yk=coastal\ region\ model}}$ are the transverse dispersion moduli, E_e is the perpendicular exchange modulus, S_e^k, D_e^k are the generation and dissipation terms of SGS energy in level-k, respectively, k′ is the Von Karman parameter, and m is the Mamayev constant (m was set to 0.75 in this study).

The model was initially running up to four months based on the parameters and data (Table 1) with a time step of 10 s, this provides output of daily and average-monthly temperatures, salinities and velocities. During the four months running, the output of each month was used as the input for the following month.

2.2. Model validation

To validate the model, instantaneous observations of temperature and salinity at X1-X13 measured by the Xiamen Environmental Protection Agency (Xiamen EPA) during the summer cruise in August 2016 were used for comparison with the output of model simulations. Root-mean-square error (RMSE, Eq. (14)) was used to characterize the degree of fit. In comparison with the coefficient of correlation (R), the Nash-Sutcliffe efficiency coefficient and the Mean absolute percentage error, RMSE is the most sensitive technique of model calibration for measuring the deviation of the residuals in the regression analysis of predicted and observed values. The lower RMSE means the better model performance. (Hyndman and Koehler, 2006; Olyaie et al., 2015).

$$\mathrm{RMSE}=\sqrt{\frac{\sum_{t=1}^{T}(Yt-Ft)^2}{T}} \tag{14}$$

where, $\mathrm{Y_t}$ is the observed value at time t, and Ft is the corresponding predicted value.

In addition, the continuous measured temperature data from monitoring of water near station X5 from the Fisheries Bureau (http://www.xmhyj.gov.cn/bmfw/hyybt/) was used to compare the model result during the four months simulation.

2.3. Simulation of the environmental fate of chemical pollutant

To test the ability of the model for predicting the spatial-temporal concentration change of chemical pollutants in the coastal water, we further assumed that 1000 kg and 1000 mg/L of a virtual chemical pollutant (no particle-reactive pollutant) leaked out from the 3-points of JR estuary named as JR North Harbor, JR Central Harbor, and JR South Harbor (point source) and whole XMB (non-point source), respectively, during the modeling period of June to September in 2016. To simplify the modeling, decomposition and/or biodegradation of the chemical pollutant was not considered in the simulation. Furthermore, we assumed that once the pollutant ran out of the boundary of XMB, the pollutant would not return to XMB. The simulation was performed day by day until the concentration change of chemical pollutant in each grid reached a concentration less than 0.01%.

3. Results and discussion

3.1. Model results

3.1.1. Results of horizontal distribution

Results of the model simulation, including average temperature, salinity and residual flow changes of the first layer in September 2016 are shown in Fig. 2, respectively, while the simulation results of the changes of average temperature, salinity and residual flow over the period of June to September of 2016 are shown in Figs. S2–S4, respectively.

Distinct changes in water temperature over time can be seen in Fig. S2. The highest temperatures were found in July and the lowest in September, with an apparent temperature range between these two months. The whole XMB had lower temperatures towards the west and higher temperatures towards the east. During the four months, the temperature gradient was obviously shown and the isotherms were compressed in June and September, while the gradient was indistinct and the isotherms had a thin disparity in July and August. Maluan Bay and Tong'an Bay showed temperature trends that were distinguished from the surrounding waters. Temperatures rose from the river mouth to the sea and from the west to the east coast during all four months, consistent with observed trends (Fig. 3 left, Fig. 4). Unlike water temperature, there was no significant fluctuation of salinity except for small wave motion in the estuarial mixed layer (Fig. S3). In July the estuary showed higher temperatures but similar salinities as the other months, which coincide with the monitoring results reported by Chen et al. (2009). The salinity values were mainly driven by ocean evaporation, rainfall, currents and river flushing, which together resulted in large diurnal variations but similar summer monthly averages. The velocity and direction of water flow in the research region is shown in Fig. S4. Two characteristic current patterns can

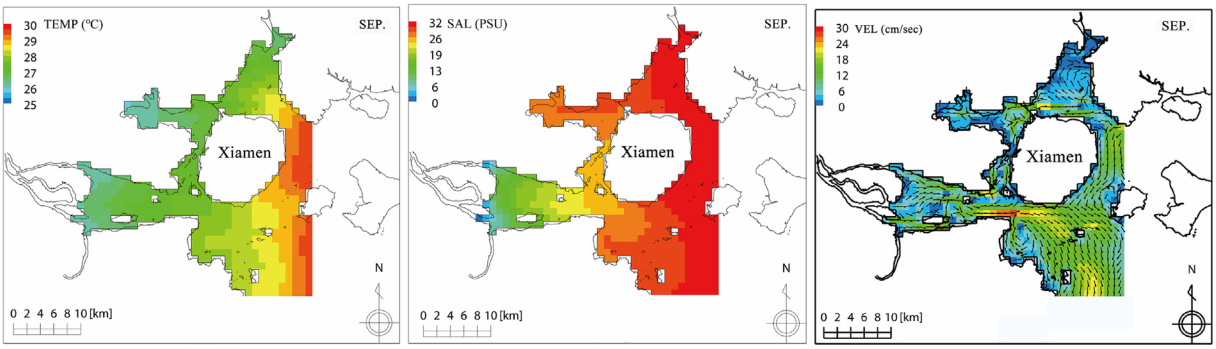

Fig. 2. Spatial distribution of average temperature, salinity and residual flow changes of the first layer in September 2016 in XMB resulted from the simulation.

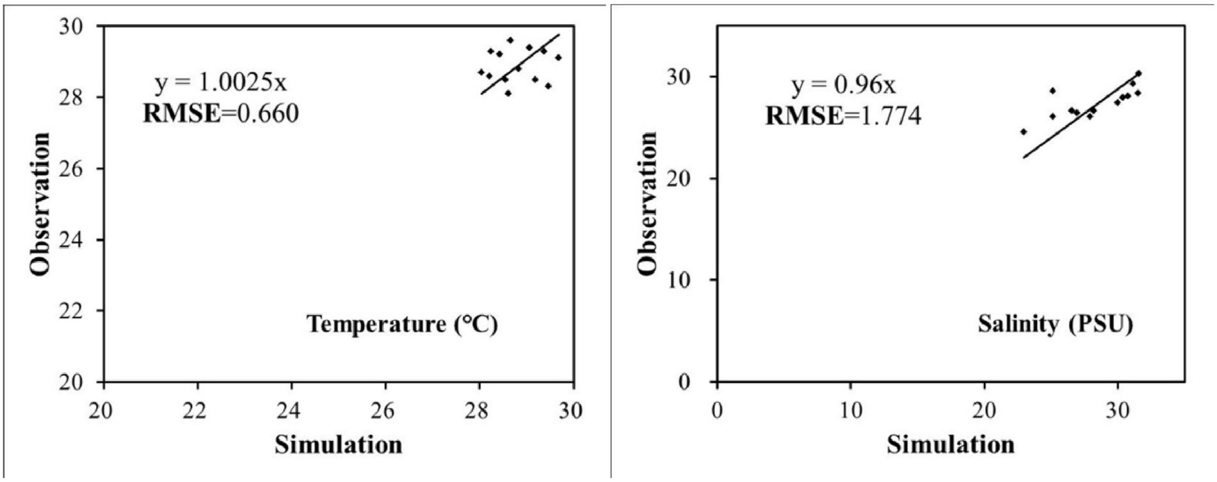

Fig. 3. Agreement between simulated and observed surface values of temperature and salinity.

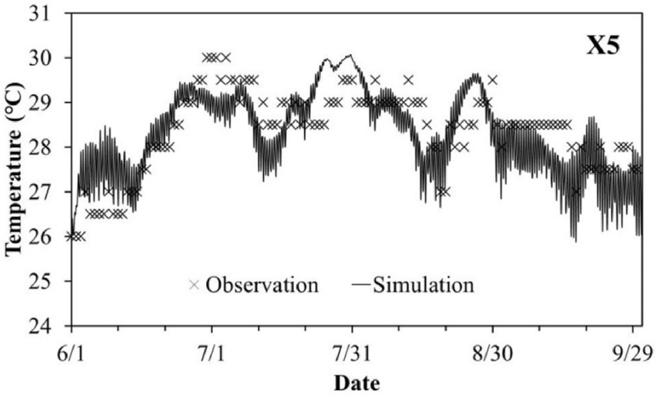

Fig. 4. Agreement between simulated and observed temperature at X5.

be seen in the model: Eastward flow in the west basin, and southward flow in southern and eastern XMB. Annual water flows are found in Maluan Bay and Tong'an Bay, controlled by topography, between Haimen Island and Jiyu Islet, the mixing zone of freshwater and seawater, around Gulangyu which is a convergence zone of estuarine water and west XMB water, and in Shuangyu where water mixes from the inner and outer bay. A cross-sectional area from X6 to X8 and the boundary region close to the sea showed particularly high flow rates. The former is the transition area from the river to the ocean, which exhibited rapid flow of deep water, and the latter is the sea area, accompanied by complex currents, density flows and offshore winds, which drive the rapid velocity of water masses.

Fig. 3 shows the validation results on temperature and salinity. Observed and modeled temperatures are symmetrical about y = 1.0025x, with values evenly distributed on both sides (Fig. 3, left). The RMSE of the linear trend was 0.660, showing good agreement between modeled and observed values of temperature. However, three reasons can most likely explain the scattered point distribution. First, the model was set to calculate the average value within the upper 5 m of water as the first layer, while during monitoring surface water was collected, which didn't exceed 0.5 m in depth. The different depths representing the 'surface' typically vary with respect to several parameters, with deeper water having a lower temperature and likely affected by ocean currents. Secondly, in the west bay, which receives anthropogenic-altered water, boundary value selection and an unpredictable mixing belt affect the results, which is why the simulation of west bay output lower temperature values than the observations, but output higher temperatures than observed in the east bay and estuary. Thirdly, on-site measurements are carried out instantaneously, which increases uncertainty. Finite monitoring data restricts the curve fitting in statistical sense, however an error of −1.2 °C–1.1 °C in temperature is acceptable and reasonable. Future monitoring data under consideration on the mentioned reasons is necessary for further improvement.

Moreover, salinity values from the simulation and observations at X1-X13 show an uneven, positive dispersion over a small sample size (Fig. 3, right). The RMSE is not as high as expected, likely attributed to the same problems as temperature. Apart from the differences between sampling and simulated depth, salinity in the estuary mixes over a wider range of end-member values, ranging from 0 to 32 from the river to the sea while temperatures only change from 24 °C to 32 °C. More importantly, temperature is mainly controlled by solar radiation, but salinity is controlled by tides, fresh water and multiple other influences, which are often more complex and difficult to accurately simulate. The three sites with the most skewed values from the trend line are X4, X5 and X6, which are all located in the mixing next to the estuary. The stations with the best fits are X10 and X11, which located in the east bay. When data from X4, X5 and X6 are removed, the RMSE value substantially decreases from 1.774 to 0.761, expressing a much better correlation. Above all, this model is superior when simulating relatively stable waters rather than acutely varying areas of the estuary.

In addition, Fig. 4 shows the comparison results between simulated and observed temperature at X5. Although variable at times, in general they show good agreement, especially during the large changes in temperature seen from July 1st to 10th and from September 9th to 19th that are likely attributable to a sudden climatological event (i.e. a typhoon).

3.1.2. *Results of vertical distribution*

As an estuarine zone, salinity in XMB is dominated by freshwater from the JR towards the west and seawater from the Taiwan strait towards the east. From Haimen Island to the Jiyu Islet is the primary mixing region of freshwater and seawater, thus we chose j = 31 as the tangent plane (Luo et al., 2012). Since salinity is not immutable over time, monthly average vertical distributions of salinity and the residual flow as the tides change are shown in Fig. S5. To clearly examine the residual flow, the arrow size was set to 50 times larger. Each model run showed the same pattern of salinity increasing towards the outer bay and with water depth. Vertically, freshwater with low salinity was found towards the surface while sea water with high salinity was found in deeper layers, forming a distinct salinity front. The current direction of water masses shows that where these salinity end-members mix, high-salinity seawater comes up from deeper water and becomes diluted by freshwater, forming a circumfluence of salinity under the surface. Horizontal mixing is similar, with the inner estuary having the lowest salinity values but exhibiting an intense gradient seaward from 10 to 25, and higher salinity close to the sea with values ranging from 28 to 32. The isohaline migrated seaward from June to September, showing that over these months freshwater gradually replaced seawater in the bay.

To further examine salinity trends from the river into the sea, we chose Site 1 (i = 24, j = 31) and Site 2 (i = 31, j = 31) as representative stations of the river mouth and mixing zone (Fig. 1), respectively, to investigate the salinity variations at each layer for each individual month (Fig. 5). On account of unequal depths at these stations, three levels of Site 1, which is in shallower water, and five levels of Site 2, which is in deeper water are given. Similarly, both sites display similar salinity increases and the low salinity layer grows deeper at similar rates. More specifically, the amplitude of salinity changes in the first three layers demonstrate that sites closer to the river where mixing occurs may show greater variations in salinity seasonally. Though slightly larger differences between these two sites were present vertically, the overall disparity among the summer months is not clear.

To build a widely adaptable model considering the maximum tide wave, the depth of the first four layers was set starting at 5 m and increased to 10 m by layer 5 to guarantee normal running. These two typical sites, representing the estuary and the sea, respectively, differ greatly in depth. In contrast with Site 1 with large spans in values and blurred layers, a clear hierarchy is embodied at Site 2. It appears that the water is in a mixed state near the estuary as Site 1 barely stages found, while a conspicuous demarcation below 10 m depth separates the river-ocean admixture and seawater like that found at Site 2. Therefore, a study investigating deep water exchange and stability of surface water can make the most of our model.

In summary of the simulation results of both the horizontal and vertical distribution, this model demonstrated a good match between observations and simulations, which underscores the feasibility of this model as a reliable model to simulate the hydrodynamic of XMB coastal water. Furthermore, this model demonstration suggests that the modeling approach of this study is applicable to other semi-closed bays when the data required for model development as shown in Table 1 is available. However, it is worth noting that for further improvement of the model, more monitoring data of XMB and some mathematical and artificial

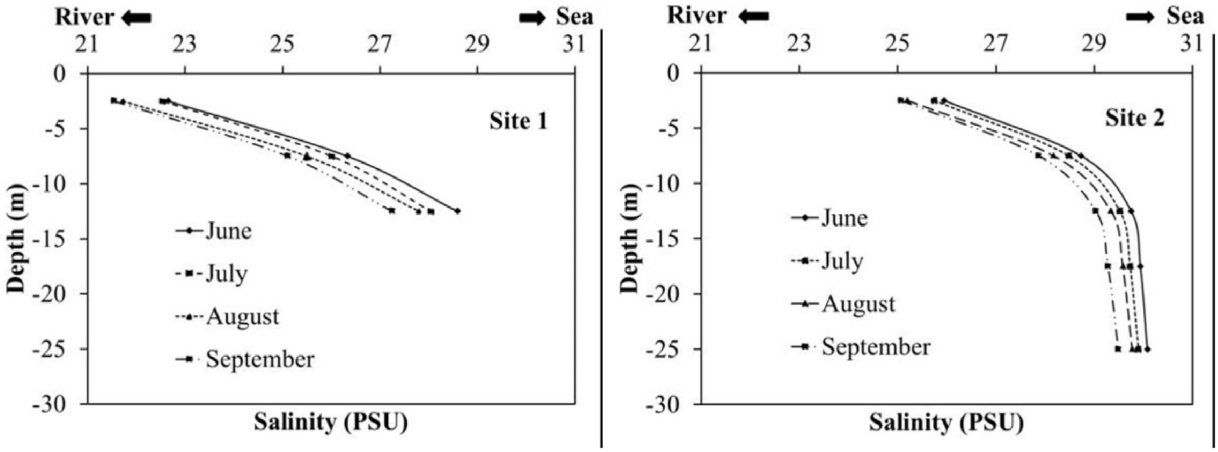

Fig. 5. Salinity distribution in layers from June to September at Site 1 and Site 2.

intelligence approaches such as data assimilation (Park and Xu, 2013), ensemble modeling (e.g., Shamshirband et al., 2019; Alizadeh et al., 2017) and artificial neural network modeling (e.g., Chen and Chau, 2016; Meng and Lin, 2008) should be considered to validate and ensure the accuracy of the model.

3.2. Simulation of chemical pollutant leaked out to XMB

3.2.1. Estuary input of pollutant (point-source)

Fig. 6 shows the simulation results of daily concentration changes in the coastal water of XMB when total 1000 kg of chemical pollutant leaked out from JR North Harbor, JR Central Harbor, and JR South Harbor. All diagrams are plotted with the same maximum percentage of 80‰ for a clear comparison. Generally, the pollutant spread rapidly under the effects of runoff and exchange with seawater. Based on the model, in the first 10 days the contaminant field expands to the whole estuary with a concentration above 80‰, more quickly to the southeast than to west XMB though still to a large degree in both directions. Remaining pollution at the harbor entrance reduced dramatically over one month. Seventy days later, no more than 16‰ resided in the whole estuary, declining at a slow rate during this period. Gradually, XMB returned to near background conditions over one hundred days. A large volume of water and exchange capacity provided the prevailing conditions in the lower estuary and the east bay to be unaffected by runoff. Conversely, dozens of days are required to regain the original state of the estuary and the west coast.

The predicted rate of pollutant loss was examined in turn to extract their distribution in time and space. Fig. S6 (left) gives exponential curves over time of remaining pollutant in the three JR harbors from north to south, whose initial removal rates rank: Central > South > North, a function of the combined effects of discharge rates and starting amounts. Trendlines showing removal at each of the three harbor locations can be characterized by the following relationships:

$$y = \begin{cases} 421.14\, e^{-0.047x} \left(R^2 = 0.989,\ \mathit{JR\ North\ Harbor}\right) \\ 283.54\, e^{-0.046x} \left(R^2 = 0.992,\ \mathit{JR\ Central\ Harbor}\right) \\ 320.69\, e^{-0.046x} \left(R^2 = 0.989,\ \mathit{JR\ South\ Harbor}\right) \end{cases}$$

where, x is the time in days and y is the concentration of the pollutant (mg/L). These equations explain the overall change in concentrations apart from the rapid loss in the first ten days. Based on the magnitude of the slopes in these equations, removal rates successively decrease in the order of North > South > Central, in

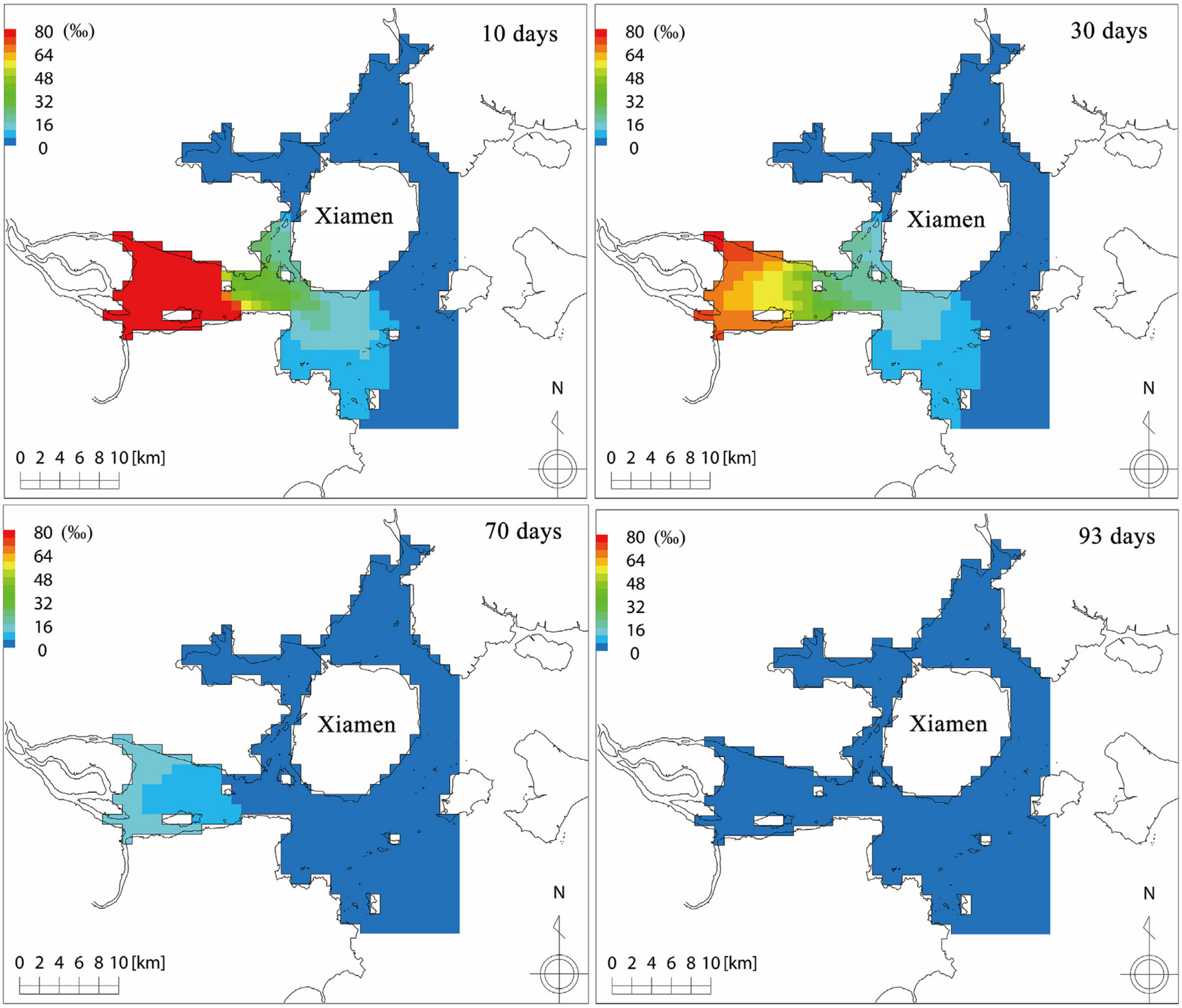

Fig. 6. The predicted spatial distribution of surface sea water in XMB (point source).

contrast with the first ten days. Additionally, it took 80, 75 and 73 days at the North, South, and Central Harbor locations, respectively, to reach pollutant levels at 0.1‰ of their starting concentrations. In other word, the three rivers each have their own elimination ability, but ones acting more dramatic at first (0–10 days) in terms of removal might exhibit more moderate rates afterwards (10 + days).

Individual points in the deep bay were surveyed as well. X6, X7 and X8, picked as part of the same latitude profile, represent a transect from the river to the sea in which all reach their highest pollutant levels of 44‰, 19‰ and 5‰, respectively, around the fifteenth day, and hardly any was found on the 120th, 110th and 90th day, respectively (Fig. S6, right). Naturally, the concentration and distance from the estuary are inversely proportional, but in light of the bends indicated, pollutant simultaneously spread at a rapid pace beyond the route limit by the force of intense flow. The case is very different at X1 in Maluan Bay, which received the pollutant on the tenth day and concentrations changed with a smooth undulating curve, presenting lower but persistent levels for three months, compared to other areas far from the estuary. This result suggested the innate shortcoming that a concave gulf causes weak-capable of water exchange.

3.2.2. *Whole XMB input of pollutant (non-point source)*

The simulate results of daily concentration changes in the coastal water of XMB when non-point source pollution of 1000 mg/L of pollutant over the entire XMB are shown in Fig. 7 and Fig. S7. As seen in Fig. 7, this circumstance is quite different from the previous point source pollutant leakage. Clearly, clues that water masses derived from upstream are useful for pushing the polluted water towards the mouth of the bay can be found, for example in eastern and southern XMB concentrations are reduced at a much faster rate than the west side, with negligible values after 30 days. Over the next four months, the east bay is removed from the pressure of the pollutant, while the west bay decreases at a slower rate. Finally, it took approximately six months for the bay water to become purified. Moreover, it is conspicuous that the two ports in Maluan Bay and Tong'an Bay, especially the former, emerges as the highest risk, followed by the west bay. In other words, though the bay purges itself half a year after a single pollution event occurs, if pollutants are input continuously such as during waste water disposal, west XMB and narrow regions of the bay will be facing a high threat. In that situation, prevention and control should be followed closely and cautiously.

From another perspective, this hypothetical simulation also accounts for the cycles and ability of water renewal. Six months is the residence time of water in a medium-sized, semi-enclosed bay such as XMB. Similar research on water exchange of the whole Bohai Bay demonstrated that a period of 580 days was typical of

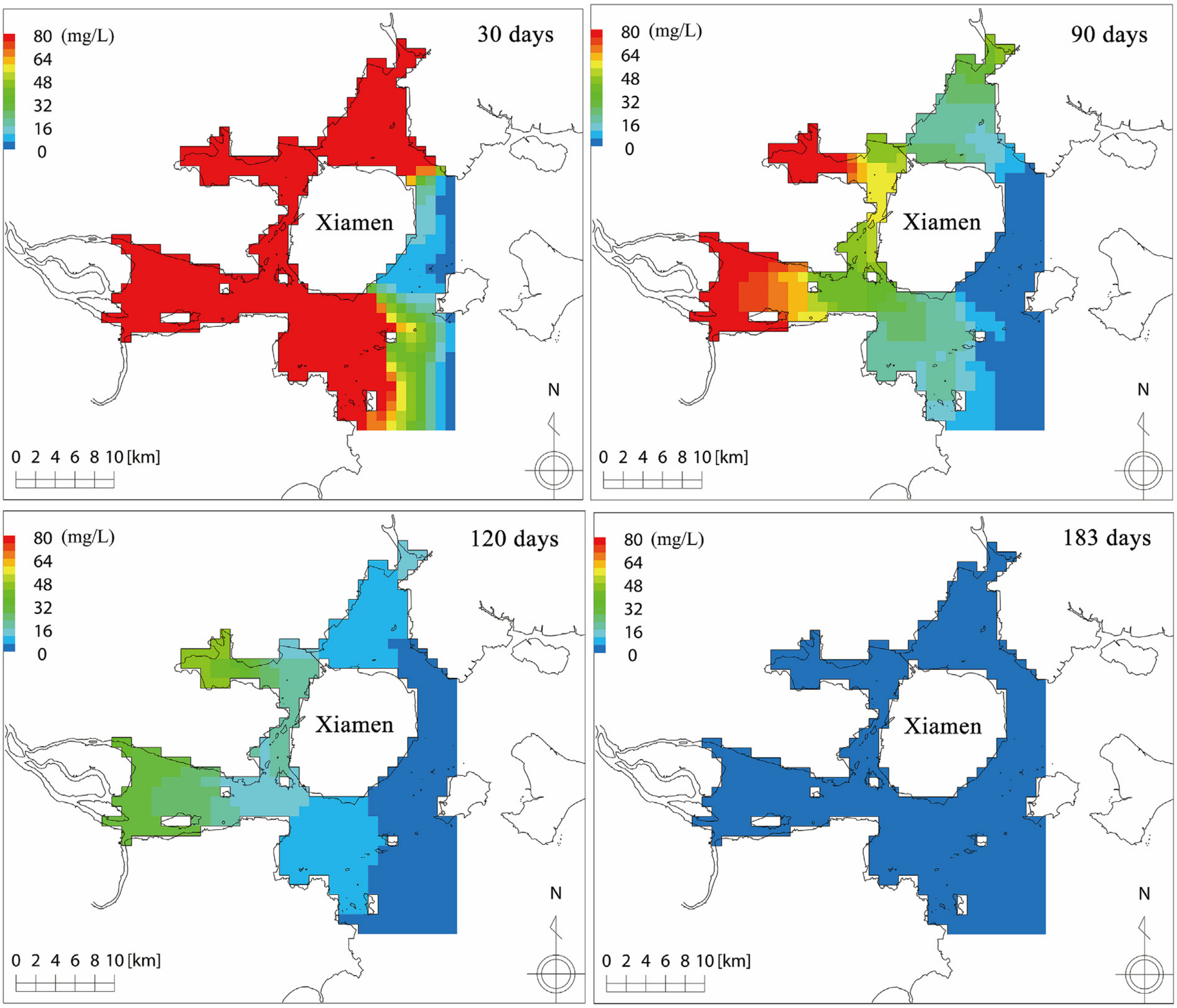

Fig. 7. The predicted spatial distribution of surface sea water in XMB (non-point source).

this switching pattern (Li et al., 2009). Another investigation utilized the radiogenic isotope ^{228}Ra to calibrate and assess the residence times in Jiaozhou Bay, on the west coast of the Yellow Sea, a much shorter time of 52 days has met the demand (Liu et al., 2004).

With respect to concentration over time (Fig. S7, left), the three JR Harbors trend show practically unanimous trendlines, which can be described by $y = 1651.1\ e^{-0.067x}(R^2 = 0.998)$. These results show that 99% of pollutants will be removed after 76 days, indicating they have the same environmental risk with dilution being only considered, resembling the whole estuary-input case. Slow arrival of external water and hampered river flow may have promoted terrace forming in the concentration vs. time plots, which explains the static 1000 mg/L value in the first half-month for the three curves, which abruptly decrease thereafter.

The order of the depuration and dilution capabilities individual sites, ranging from the highest to the slowest rates, was X8>X7>X6>X1, which progressively decrease in proximity to the sea and cabined gulf in proper order in Fig. S7 (right). The formulated dynamic expression of second section is

$$y = \begin{cases} 1397.5\ e^{-0.067x}\left(R^2 = 0.999,\ X1\right) \\ 969.74\ e^{-0.07x}\left(R^2 = 0.999, X6\right) \\ 640\ e^{-0.071x}\left(R^2 = 0.997, X7\right) \\ 228.15\ e^{-0.072x}\left(R^2 = 0.993, X8\right) \end{cases}$$

The time it took to reduce the pollutant concentrations to 1% were 74, 66, 59 and 44 days for X1, X6, X7 and X8, respectively. However, the gradient ratio stands at the reverse side of occasion at the outset, to get the result of clearing the pollutant in a similar time, describing that the ocean not only purifies itself, but also takes the incoming river by tidal forcing. With no consideration of biological factors, the decreasing removal rate is associated with water mass quantity and local topography to a large degree. X8 is located at a position with considerable water volume and a wide terrain, linking X7 to X6 with a small flow of water, while X1 standing in the depression disadvantage. From this profile, a conclusion can be drawn that closer to the sea, the exchange rates of water masses and the removal of pollutant will increase.

In summary, this virtual simulation of chemical pollutant clearly demonstrates the capability and the usefulness of XMB hydrodynamic model. Even it was a preliminary trial and further improvement of the model is necessary, the results suggest that model simulation can easily and quickly provide valuable information for people to take measures when accidental chemical spills happen, such as recently happened at Quanzhou Harbor, Fujian, China.

4. Conclusions

A 3D hydrodynamic model for predicting the environmental fate of chemical pollutants in XMB was demonstrated in this study. Temporal and spatial (horizontal and vertical) distributions of temperature, salinity and flow field were obtained through model simulations. The simulations coincided with the observations in most circumstances, which is a favorable consequence with the limited observational sample size. Furthermore, results from model simulation of a virtual chemical pollutant leaked out from JR estuary (point source) and whole XMB (non-point source), respectively, shows that three and six months, respectively, were required for the bay waters to flush themselves of the pollutant, and sites with a narrow terrain (west XMB) had a high residual risk. To further improve the hydrodynamic model, multiple-layer and wider-coverage monitoring observations, modeling approaches such as data assimilation and artificial neural network are necessary to be considered, which will foster prediction with high precision and further in-depth research on environmental fate of chemical pollutant as well.

Acknowledgement

This study was supported by National Natural Science Foundation of China (Grant No: 41877474 , 41576115) and National Marine Hazard Mitigation Service, China, also funded by National Institute of Advanced Industrial Science and Technology (AIST) during October 20th, 2016 to January 16th, 2017 and September 1st, 2017 to March 21st, 2018. WEL Visiting Fellowship Program of the Key Laboratory of the Coastal and Wetland Ecosystems (Xiamen University), Ministry of Education also made contribution to this study.

Appendix A. Supplementary data

Supplementary data to this article can be found online at https://doi.org/10.1016/j.envpol.2019.113000.

References

Alizadeh, M.J., Nodoushan, E.J., Kalarestaghi, N., Chau, K.W., 2017. Toward multi-day-ahead forecasting of suspended sediment concentration using ensemble models. Environ. Sci. Pollut. Control Ser. 24 (36), 28017–28025. https://doi.org/10.1007/s11356-017-0405-4.

Cai, M., Hong, Q., Sun, J., Sundqvist, K., Wiberg, K., Chen, K., Wang, Y., Qiu, C., Huang, S., 2016. Concentrations, distribution and sources of polychlorinated dibenzo-p-dioxins and dibenzofurans and dioxin-like polychlorinated biphenyls in coastal sediments from Xiamen, China. Mar. Chem. 185, 74–81. https://doi.org/10.1016/j.marchem.2016.05.008.

Chau, K.W., 2005. Characterization of transboundary POP contamination in aquatic ecosystems of Pearl River delta. Mar. Pollut. Bull. 51 (8–12), 960–965. https://doi.org/10.1016/j.marpolbul.2005.02.028.

Chen, X.Y., Chau, K.W., 2016. A hybrid double feedforward neural network for suspended sediment load estimation. Water Resour. Manag. 30 (7), 2179–2194. https://doi.org/10.1007/s11269-016-1281-2.

Chen, X.H., Hu, J.Y., Pi, Q.L., Liu, G.P., Chen, Z.Z., 2009. Densely underway measurement of surface temperature and salinity in Xiamen-Quanzhou near-shore area. Adv. Earth Sci. 24, 629–635. https://doi.org/10.3321/j.issn:1001-8166.2009.06.008 (in Chinese).

Chen, B.H., Ji, W.D., Chen, J.M., Lin, C., Huang, H.N., Huo, Y.L., Ji, X.B., 2013. Characteristics of nutrients in the Jiulong River and its impact on Xiamen water, China. Chin. J. Oceanol. Limnol. 31, 1055–1063. https://doi.org/10.1007/s00343-013-2263-3.

Grung, M., Lin, Y., Zhang, H., Steen, A.O., Huang, J., Zhang, G., Larssen, T., 2015. Pesticide levels and environmental risk in aquatic environments in China - a review. Environ. Int. 81, 87–97. https://doi.org/10.1016/j.envint.2015.04.013.

Hao, Q., Sun, Y.X., Xu, X.R., Yao, Z.W., Wang, Y.S., Zhang, Z.W., Luo, X.J., Mai, B.X., 2015. Geographical distribution and risk assessment of persistent organic pollutants in golden threads (Nemipterus virgatus) from the northern South China Sea. Ecotoxicology 24, 1593–1600. https://doi.org/10.1007/s10646-015-1475-z.

Homami, M., Mirbagheri, S.A., Borghei, S.M., Abbaspour, M., 2017. Simulation modeling of nutrients, dissolved oxygen and total dissolved solids in peer-bazar river and anzali wetland eutrophication prediction. Desalin. Water Treat 79, 108–124. https://doi.org/10.5004/dwt.2017.20704.

Horiguchi, F., Yamamoto, J., Nakata, K., 2001. A numerical simulation of the seasonal cycle of temperature, salinity and velocity fields in Tokyo bay. Mar. Pollut. Bull. 43, 145–153. https://doi.org/10.1016/s0025-326x(01)00116-3.

Hyndman, R.J., Koehler, A.B., 2006. Another look at measures of forecast accuracy. Int. J. Forecast. 22, 679–688. https://doi.org/10.1016/j.ijforecast.2006.03.001.

Data assimilation for atmospheric, oceanic and hydrologic applications. In: Park, Seon Ki, Xu, Liang (Eds.), 2013. New Theories and Methodologies in Data Assimilation, Vol. II. Springer-Verlag. ISBN 978-3-642-35087-0.

Kim, N.-H., Hwang, J.H., Cho, J., Kim, J.S., 2018. A framework to determine the locations of the environmental monitoring in an estuary of the Yellow Sea. Environ. Pollut. 241, 576–585. https://doi.org/10.1016/j.envpol.2018.05.097.

Kobayashi, N., Eriguchi, T., Nakata, K., Masunaga, S., Horiguchi, F., Nakanishi, J., 2006. Application of a 3-D chemical fate prediction model (FATE3D) to predict dioxin concentrations in the Tokyo Bay. Estuar. Coast. Shelf Sci. 70, 621–632. https://doi.org/10.1016/j.ecss.2006.06.013.

Li, X.B., Yuan, D.K., Sun, J., 2009. Simulation of water exchange in Bohai bay. Adv. Water Resour. Hydraul. Eng. 1341–1346. https://doi.org/10.1007/978-3-540-89465-0.

Li, J., Huang, Z.Y., Hu, Y., Yang, H., 2013. Potential risk assessment of heavy metals by consuming shellfish collected from Xiamen, China. Environ. Sci. Pollut. Res. 20, 2937–2947. https://doi.org/10.1007/s11356-012-1207-3.

Lin, H.Y., Chen, Z.Z., Hu, J.Y., Cucco, A., Zhu, J., Sun, Z.Y., Huang, L.F., 2017. Numerical simulation of the hydrodynamics and water exchange in Sansha Bay. Ocean Eng. 139, 85–94. https://doi.org/10.1016/j.oceaneng.2017.04.031.

Liu, Z., Wei, H., Liu, G.S., Zhang, J., 2004. Simulation of water exchange in Jiaozhou Bay by average residence time approach. Estuar. Coast Shelf Sci. 61, 25–35. https://doi.org/10.1016/j.ecss.2004.04.009.

Liu, R., Zhang, X.Q., Liang, B.C., Xin, L., Zhao, Y., 2017. Numerical study on the influences of hydrodynamic factors on water age in the Liao River estuary, China. J. Coast. Res. 80, 98–107. https://doi.org/10.2112/SI80-014.1.

Luo, Z.B., Pan, W.R., Li, L., Zhang, G.R., 2012. The study on three-dimensional numerical model and fronts of the Jiulong Estuary and the Xiamen Bay. Acta Oceanol. Sin. 31, 55–64. https://doi.org/10.1007/s13131-012-0220-1.

Meng, Yaobin, Lin, Bin-Le, 2008. A feed forward artificial neural network for prediction of aquatic ecotoxicity of alcohol ethoxylate. Ecotoxicol. Environ. Saf. 71 (2008), 172–186. https://doi.org/10.1016/j.ecoenv.2007.06.011.

Olyaie, E., Banejad, H., Chau, K.-W., Melesse, A.M., 2015. A comparison of various artificial intelligence approaches performance for estimating suspended sediment load of river systems: a case study in United States. Environ. Monit. Assess. 187 https://doi.org/10.1007/s10661-015-4381-1.

Periáñez, R., 2009. Environmental modelling in the Gulf of Cadiz: heavy metal distributions in water and sediments. Sci. Total Environ. 407, 3392–3406. https://doi.org/10.1016/j.scitotenv.2009.01.023.

Qian, Z.Z., Luo, F.F., Wu, C.Y., Zhao, R., Cheng, X., Qin, W.F., 2017. Indicator polychlorinated biphenyls (PCBs) and organochlorine pesticides (OCPs) in seafood from Xiamen (China): levels, distributions, and risk assessment. Environ. Sci. Pollut. Res. 24, 10443–10453. https://doi.org/10.1007/s11356-017-8659-4.

Shamshirband, S., et al., 2019. Ensemble models with uncertainty analysis for multiday ahead forecasting of chlorophyll a concentration in coastal waters. Eng. Appl. Comput. Fluid Mech. 13 (1), 91–101. https://doi.org/10.1080/19942060.2018.1553742, 2019.

Wang, Z.F., Wu, K.J., Gao, S.H., Li, Q.J., 2017. Nearshore wave forecast for Xiamen, China. J. Coast. Res. 80, 48–54. https://doi.org/10.2112/SI80-008.1.

Yuan, D., Yang, D., Wade, T.L., Qian, Y., 2001. Status of persistent organic pollutants in the sediment from several estuaries in China. Environ. Pollut. 114 (1), 101–111. https://doi.org/10.1016/S0269-7491(00)00200-1.

Zhai, X.Y., Xia, J., Zhang, Y.Y., 2017. Integrated approach of hydrological and water quality dynamic simulation for anthropogenic disturbance assessment in the Huai River Basin, China. Sci. Total Environ. 598, 749–764. https://doi.org/10.1016/j.scitotenv.2017.04.092.